Journal of Materials Chemistry A

Accepted Manuscript

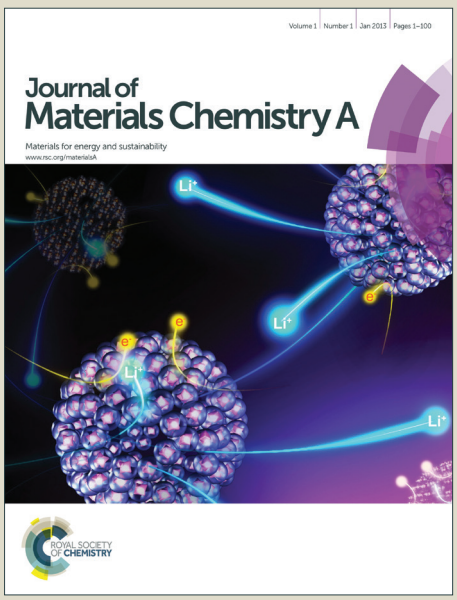

ROYAL SOCIETY OF CHEMISTRY

www.rsc.org/materialsA

Cite this: DOI: 10.1039/c0xx00000x

www.rsc.org/xxxxxx

ARTICLE TYPE

MoS_2 nanosheet/Mo_2C-embedded N-doped carbon nanotubes: Synthesis and electrocatalytic hydrogen evolution performance†

Kai Zhang,[a] Yang Zhao,[a] Shen Zhang, Hailong Yu,[a] Yujin Chen, *[a] Peng Gao, *[b] and Chunling Zhu*[b]

Received (in XXX, XXX) Xth XXXXXXXXX 20XX, Accepted Xth XXXXXXXXX 20XX

DOI: 10.1039/b000000x

***In situ* solid and subsequent hydrothermal reactions were developed to grow ultrathin MoS_2 nanosheets on Mo_2C-embedded N-doped carbon nanotubes. As applied as electrocatalyts for hydrogen evolution, the hybrid nanotubes exhibited excellent catalytic activity.**

Hydrogen, as a green fuel, is a promising candidate for traditional petroleum fuels in the future. The rare metals, such as platinum, have high efficiency in the hydrogen evolution reaction (HER), however, their high cost and scarcity limit their large scale applications. During the past few years, MoS_2 has attracted much attention due to its high abundance, low cost and chemical stability in the acid solution. Density functional theory calculations indicated that the edges of MoS_2 nanoparticles were active for hydrogen evolution, while their (0001) basal planes were catalytically inert.[1] In terms of subsequent experimental results, T. F. Jaramillo and his coworkers demonstrated that the electrocatalytic activity for hydrogen evolution of MoS_2 correlated linearly with the number of edge sites on the MoS_2 catalyst.[2] Thereafter, enormous efforts have been put into optimizing MoS_2 nanostructures to increase the amount of edges per mole MoS_2.[3] As a result, the electrocatalytic performances of those optimized MoS_2 nanostructures were significantly improved. For example, the Tafel slope of highly ordered double-gyroid MoS_2 bicontinous networks was as low as 50 mV per decade.[3b] Besides the aspect of active sites, another issue need to be also addressed well when MoS_2 nanostructures applied for HER catalyst, i. e., an extremely low conductivity between two adjacent van der Waals bonded S–Mo–S sheets.[4, 5] Resistivity through the basal planes has been measured to be 2200 times larger than that through the direction parallel to the planes, which significantly decreases the overall HER rate.[5a] Such low conductivity great limits charge transfer rate during the HER process, and consequently suppresses the total HER efficiency of MoS_2 nanostructures. One efficient way to solve the problem is growing MoS_2 nanostructures on conductive substrates, such as graphene, graphite, and carbon paper, etc.[6] In this case, an advantageous catalyst design may be to make (0001) basal planes of MoS_2 nanostructures perpendicular to the conductive surface.[5a] However, most of the conductive substrates are inert for HER, which significantly decreases the density of active sites of MoS_2 nanostructures. Thus, increasing both the conductivity and active sites of MoS_2 nanostructures simultaneously for efficient HER electrocatalysts still remains a challenging task.

In this work, we describe a strategy based on *in situ* solid reaction and subsequent hydrothermal reactions to grow MoS_2 nanosheets on N-doped carbon nanotubes (NCNTs) with Mo_2C nanoparticles embedded in the NCNT walls. Compared with other MoS_2 based heteronanostructures, the synthesized MoS_2 composite applied as HER catalyst offers the following advantages: (i) The composites posses abundant active sites for HER because the thickness of MoS_2 nanosheets is in range of 1–5 nm, and the MoS_2 nanosheets grown on the surface of N-doped carbon nanotubes with an angle that allows more active edge sites exposed to electrolyte. Besides, the spacing (002) of the basal planes of MoS_2 nanosheets are expanded. This leads to rich-defect in MoS_2 nanosheets, which provides additional active edge sites for HER.[3f, g] (ii) NCNT in the composite can significantly improve the whole conductivity of the electrocatalyst, and thus increases charge transfer rate during the HER process.[5a] (iii) Mo_2C nanoparticles are active for HER,[7] and thus the introduction of NCNTs in the composite would not decrease the density of the active sites of the electrocatalyst significantly.

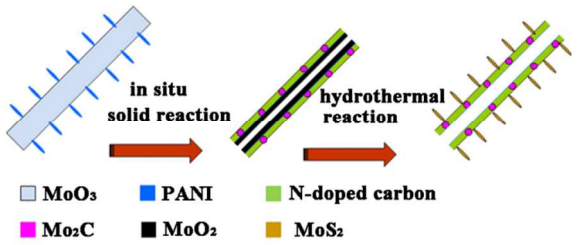

Scheme 1 Illustration of the growth processes of MoS_2/Mo_2C-NCNTs.

The growth of MoS_2 nanosheets on Mo_2C-embedded NCNTs (named as MoS_2/Mo_2C-NCNTs for convenience) is based on *in situ* solid and subsequent hydrothermal reactions, as illustrated in Scheme 1. MoO_3/polyaniline (MoO_3/PANI) hybrids were first fabricated by our previous method with a modification.[8] After the hybrids were annealed at 700°C for 2 h under an Ar flow, interesting tube-like nanostructures were obtained, in which the inner and outer walls consist of MoO_2 and amorphous N-doped carbon material with crystalline Mo_2C nanoparticles embedded in the carbon material, respectively (for convenience, this product is named as MoO_2/Mo_2C-NCNTs). Under a hydrothermal condition with the presence of thiourea, MoO_2/Mo_2C-NCNTs can be transformed into MoS_2/Mo_2C-NCNTs at 200°C for 48 h. The detailed synthesis processes are also described in the Electronic

Supplementary Information (ESI).†

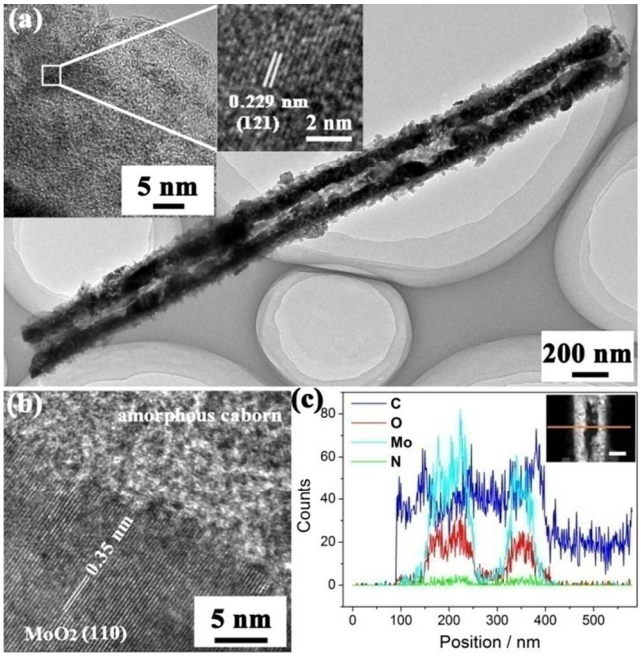

Fig. 1 Structural characterization of MoO_2/Mo_2C-NCNTs. (a) TEM image, the left inset showing amorphous N-doped carbon layer, and the right inset showing HRTEM image of crystalline Mo_2C embedded in amorphous carbon layer, (b) HRTEM, and (c) EELS spectrum.

PANI has been demonstrated to be able to grow readily on the surfaces of various inorganic materials as various forms, such as nanorods, nanoparticles, and thin films, if the polymerization conditions are controlled properly. [8, 9] In the present work, by tuning polymerization temperature and the concentration of aniline, PANI thin films were uniformly coated on the MoO_3 nanowires. The as-synthesized products were examined by scanning electron microscopy (SEM) and transmission electron microscopy (TEM). A typical SEM image (**Fig. S1)** clearly shows that MoO_3/PANI hybrids were synthesized in high yields with lengths and diameters of about several micrometers and 400 nm, respectively.† An *in situ* solid reaction for the formation of MoO_2/Mo_2C-NCNTs was carried out by heating the MoO_3/PANI hybrids at 700°C for 2 h at an Ar atmosphere. X-ray diffraction (XRD) (**Fig. S2**) reveals that the products contain crystalline Mo_2C (JCPDs PDF no. 77-0720) and MoO_2 (JCPDs PDF no.86-0135).† SEM image (**Fig. S3**) shows that the diameter of the open MoO_2/Mo_2C-NCNTs decreases down to about 320 nm.† A low-magnification TEM image (**Fig. 1(a)**) clearly demonstrates that the thickness of the walls the hybrid NCNTs are about 135 nm. From the TEM image, light and dark regions can also be identified in the walls of the hybrid NTs, implying that the hybrid NTs are composed of different materials. The lattice distance in the dark region (inner wall) from high-resolution TEM (HRTEM) image (**Fig. 1(b)**) is 0.35 nm, corresponding to (110) crystal plane of MoO_2. It suggests that MoO_3 is reduced into MoO_2 by polyaniline during the solid reaction process. At the most areas of the outer walls of the hybrid NTs no lattice fringes are observed, however, small embedded particles are identified (the left inset in **Fig. 1(a)**). HRTEM image (the right inset in **Fig. 1(a)**) shows that the lattice distance from the small particles is 0.229 nm, corresponding to (121) plane of Mo_2C. The XRD and TEM analyses show that the inner wall of the NTs is MoO_2, and the outer wall is composed of amorphous carbon material and crystalline Mo_2C. In order to further determine the composition of the hybrid nanotubes, line-scan electron energy loss spectroscopy (EELS) was carried out, as shown in **Fig. 1(c).** It can be clearly found that the C and N elements are distributed in the whole regions of the NTs, whereas the Mo and O elements are mainly distributed in the inner walls. X-ray photoelectron spectroscopy (XPS) further confirms the presence of N element in the NTs, and its percentage is determined to be 20 at% **(Fig. S4)**.† On one hand, the results above further confirms the tubular character of the products; on the other hand, it demonstrates that the outer wall is composed of N-doped and Mo_2C embedded-amorphous carbon material, and the inner wall is crystalline MoO_2.

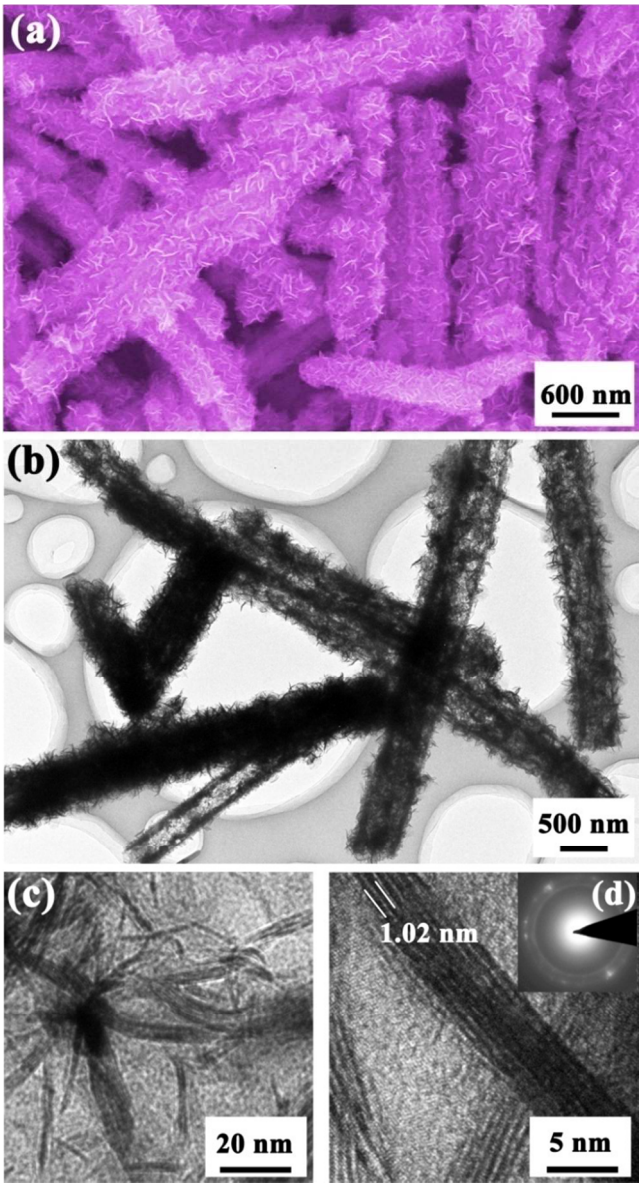

Fig. 2 Structural characterization of MoS_2/Mo_2C-NCNTs. (a) SEM, (b, c) TEM, and (d) HRTEM images, the inset in (d) showing SAED pattern of basal plane of MoS_2 nanosheets.

These results above imply that the interesting MoO_2/Mo_2C-NCNTs can be successfully obtained by the simply annealing of the MoO_3/PANI hybrids at an Ar atmosphere. The formation of the tubular structures is similar to those of hollow inorganic nanocrystals based on a method through the nanoscale Kirkendall effect.[10] The key process for hollow structure preparation through the nanoscale Kirkendall effect is the formation of a so-called "core–shell" structure at the initial stage. A net vacancy diffusion towards the interior with the reaction process processed if the diffusion of core material is faster than that of the shell material, which gradually leads to void space at the core–shell interface, and eventually the formation of a hollow structure. In the present work, both MoO_3 and PANI are instable thermodynamically. At a high temperature, the diffusion rate of MoO_3 core is faster than that of the PANI shell. With the chemical reaction between MoO_3 and PANI proceeded, most of MoO_3 material was reduced into MoO_2 phase, accompanying with the formation of a hollow region in the center of the products. Due to its faster diffusion rate MoO_3 would further diffuse through the core-shell interfaces into shell region, and react with PANI. Consequently, produced Mo_2C nanoparticles would be embedded in the outer wall of the NCNTs. It is worth noting that the N elements in PANI cannot be removed completely at the temperature of 700°C, which leads to *in situ* N-doping in the outer walls of the hybrid NTs.

The hydrothermal reaction for the preparation of MoS_2/Mo_2C-NCNTs was carried out by heating an aqueous solution contains the MoO_2/Mo_2C-NCNTs as precursors and thiourea as the sulfur source at 200°C for 48 h. During the heating process, O^{2-} ions in MoO_2/Mo_2C-NCNTs were replaced with S^{2-} ions, leading to the transformation of MoO_2 to MoS_2. XRD technique was conducted to investigate the structural information of the product. As shown in **Fig. S5**, besides the diffraction peaks indicated by "*" from Mo_2C, several ones from MoS_2 marked by "#" are also found in the XRD pattern.† Two broadened peaks at high-angle region (32.7 and 58.3°) are well indexed to (100) and (110) planes of 2H-MoS_2 (JCPDS 37-1492). This indicates the crystalline MoS_2 and Mo_2C are presented in the product. It is noteworthy that the diffraction peak of 2H-MoS_2 at 2θ=14.4° shifts to low-angles of 2θ=8.5 and 13.8°, suggesting that the interlayer distance of (002) plane of MoS_2 is expanded.[11] Using the Bragg equation, the corresponding expanded d spacings are 1.04 and 0.64 nm, respectively. Moreover, all of the diffraction peaks from MoS_2 are broadened, suggesting its low crystallinity. In addition, the small peak at 2θ=26.0 corresponds to (011) plane of MoO_2, suggesting that small parts of MoO_2 still present in the final product. The structure of the MoS_2/Mo_2C-NCNTs is further characterized by SEM and TEM observations. SEM image (**Fig. 2(a)**) shows the MoS_2/Mo_2C-NCNTs have interesting hierarchical morphologies, i.e., many ultrathin nanosheets grown almost perpendicularly on the surfaces of one-dimensional nanostructures. The lengths and diameters of MoS_2/Mo_2C-NCNTs are about 3.5 μm and 500 nm, respectively. The low-resolution TEM image (**Fig. 2(b)**) reveals that the products are still of tubular character with the ultrathin nanosheets surrounding outside. The cross-sectional TEM image (**Fig. 2(c)**) reveals that the thickness of MoS_2 nanosheets is in the range of 1–5 nm. In the corresponding HRTEM image (**Fig. 2(d)**), most of the edges of MoS_2 nanosheets have large spacing of 1.02 nm**,** which is consistent with the result from XRD analysis. The corresponding selected-area electron diffraction (SAED) (the inset in **Fig. 2(d)**) of the basal plane of MoS_2 nanosheets show that the atomic arranging manners on the basal surfaces are disordered. As previously demonstrated, the expanded spacings of (002) plane were attributed to oxygen incorporation in MoS_2. [3] First-principle calculations and experimental data further proved that the oxygen incorporation could effectively regulate the electronic structure, improved the intrinsic conductivity of MoS_2, and consequently enhanced its HER activity significantly.

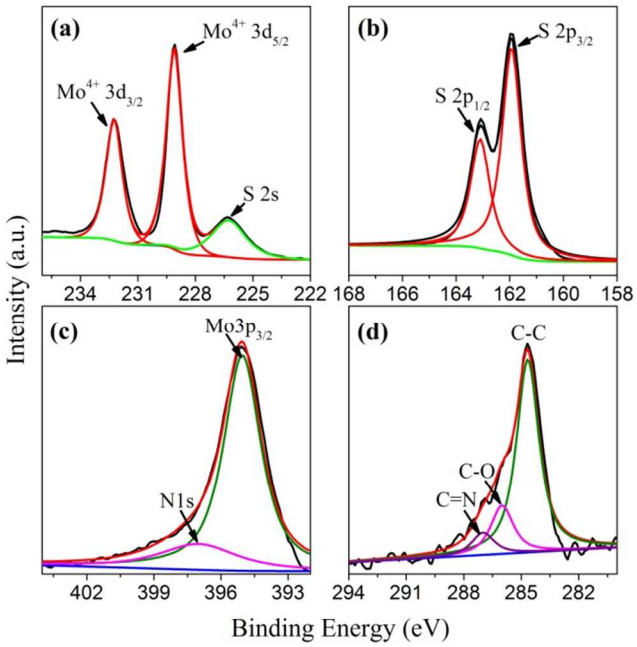

Fig. 3 XPS spectra of MoS_2/Mo_2C-NCNTs. (a) Mo 3d, (b) S 2p, (c) N 1s, and (d) C 1s spectrra.

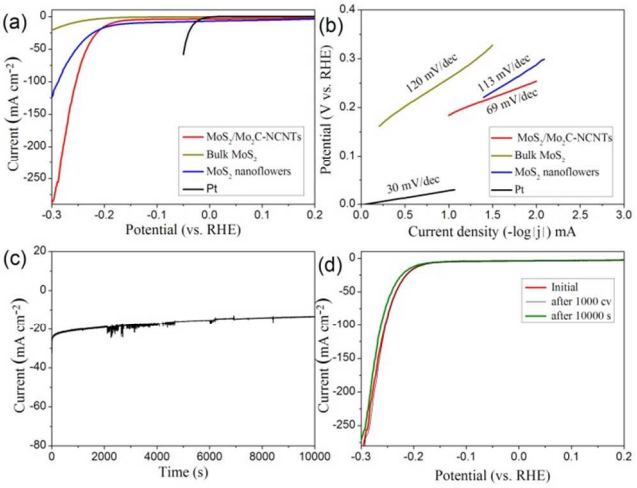

Figure 4. (a) Polarization curves, and (b) Tafel plots of Pt, bulk MoS_2, MoS_2 nanoflowers, and MoS_2/Mo_2C-NCNTs, (c) Cycling stability of MoS_2/Mo_2C-NCNTs at an overpotential of 220 mV, and (d) Polarization curves showing that negligible degradation of HER activity of MoS_2/Mo_2C-NCNTs after 1000 cycles and continuous hydrogen production for 10,000 s at an overpotential of 220 mV.

The surface electronic state and composition of the MoS_2/Mo_2C-NCNTs were further investigated by X-ray

photoelectron spectroscopy (XPS). The survey XPS spectrum (**Fig. S6**) indicates that the NTs are composed of the C, Mo, S, and O elements.† **Fig. 3(a)** shows a high-resolution spectrum in the binding energy range of 222–236 eV. The Mo 3d peaks located at 229.1 and 232.2 eV have a spin energy separation of 3.1 eV, characteristic doublet of core-level of $Mo^{(IV)}$ oxidation state in MoS_2.[3a] The peak at around 226.3 eV corresponds to the S 2s component of MoS_2. In the high-resolution S 2p region (**Fig. 3(b)**), the peaks at 161.9 and 163.1 eV are observed, corresponding to S $2p_{3/2}$ and S $2p_{1/2}$, respectively. The intensity ratio of the two peaks is about 2:1, and their energy is about 1.2 eV, a characteristic of S^{2-} species.[11] the peak at 397.0 eV in **Fig. 3(c)** can be attracted to N 1s component, while the peak at 395.1 corresponds to Mo $3p_{3/2}$. **Fig. 3(d)** shows the standard carbon peak at 284.6 eV, in which the asymmetric peak indicates that C–O (at 286.0 eV) and C=N (at 287.0 eV) groups exist in the surfaces of amorphous carbon materials. The EELS spectrum for MoS_2/Mo_2C-NCNTs further confirms that the hybrid nanotubes contain C, Mo, S, and N elements, as shown in Fig. S7.

Electrochemical measurements of the MoS_2/Mo_2C-NCNTs loaded on carbon paper as well as Pt, bulk MoS_2 and MoS_2 nanoflowers were carried out in 0.5 M H_2SO_4 solution using a three-electrode setup to evaluate their HER activities.† MoS_2 nanoflowers were fabricated by a hydrothermal method, and the synthesized process and structural characterization are described in ESI (**Fig. S8**).† As shown in **Fig. 4(a)**, compared to the bulk MoS_2 and MoS_2 nanoflowers, the MoS_2/Mo_2C-NCNTs exhibit much lower onset overpotential (η) of 145 mV, suggesting the superior HER activity of the hybrid NCNTs. Furthermore, the cathodic current density (J) of the hybrid NTs is 280 mA cm^{-2} at η= 300 mV, which is 13 and 2.3 times than the current density of bulk MoS_2 and MoS_2 nanoflowers. Notably, the cathodic current density of the hybrid NTs is also larger than those of other MoS_2, MoS_2-based and Mo_2C-based nanostructures. [3b, 3f, 3g, 6a, 7a, 12, 13] This further confirms superior catalytic activity of the hybrid NCNTs for HER. The large current density means prominent hydrogen evolution behavior, evidenced by the continuous and small bubbles escaped from the hybrid NCNT electrode surfaces (video, ESI).† **Fig. 4(b)** shows the Tafel slopes for the tested samples. The Tafel slope of the hybrid NTs (69 mV $decade^{-1}$) is lower than those of bulk MoS_2 (120 mV $decade^{-1}$) and MoS_2 nanoflowers (113 mV $decade^{-1}$). Although the Tafel slope is larger than those of some other nanostructured MoS_2, it exhibits the largest exchange current density (21 μA cm^{-2}), as shown in **Table S1**. Therefore, the MoS_2/Mo_2C-NCNTs have excellent HER activity. The good HER behavior of the NTs is related to the following factors. (i) Ultrathin thickness (1-5 nm) and the expanded spacing of (002) plane result in more abundant active sites for HER. [3f, 3g] (ii) Mo_2C nanoparticles are active for HER,[7] and thus the introduction of NCNTs in the composite would not decrease the density of the active sites of the electrocatalyst significantly. (iii) NCNT in the composite can significantly improve the whole conductivity of the electrocatalyst, and thus increases charge transfer rate during the HER process.[4, 5a] The electrochemical impedance spectroscopy shows that the charge transfer resistance of MoS_2/Mo_2C-NCNTs (**1.9 Ω**) is smaller than that of MoS_2 nanoflowers (**2.2 Ω**), as shown in **Fig. S9**. (iv) The MoS_2 nanosheets are grown vertically on the surface of the NCNTs, and thus there is void space between the neighboring nanosheets, as shown **Fig. 2(a)**. Compared to other types of MoS_2 films, the hybrid NCNT electrodes allow more active sites for HER to contact with electrolyte, which is helpful to the improvement of the overall efficiency of HER.

To investigate the stability during HER process, a long-term cycling test and continuous HER at a given overpotential were carried out. As shown in **Fig. 4(c)**, as an overpotential of 220 mV was applied, the MoS_2/Mo_2C-NCNTs exhibited a continuous HER behavior. After a period of 10,000 seconds, the cathodic current density has very little degradation. The negligible difference in the polarization curves measured before and after 1,000 cycles at a scan rate of 100 mV s^{-1}, and continuous hydrogen production for 10,000 seconds at an overpotential of 220 mV further confirms the long-term electrochemical stability, as shown in **Fig. 4(d)**.

Conclusions

We develop in situ solid reaction and subsequent hydrothermal reactions to grow ultrathin MoS_2 nanosheets with ultrathin thickness on the surfaces of N-doped and Mo_2C-embedded carbon nanotubes. As applied as cathode electrode for electrocatalytic HER, the hybrid NTs exhibit excellent HER activity with small onset overpotential of 145 mV, a large exchange current density of 21 μA cm^{-2}, and a large cathodic current density of 280 mA cm^{-2} at η= 300 mV due to more active edge sites for HER and very high conductivity of carbon nanotubes. Our results demonstrate that the NTs are very promising for HER electrocatalysts.

Acknowledgements

We thank the National Natural Science Foundation of China (Grant Nos. 51272050 and 21271053), the Innovation Foundation of Harbin City (2012RFXXG096), and also the 111 project (B13015) of Ministry Education of China to the Harbin Engineering University.

Notes and references

[a] *Key Laboratory of In-Fiber Intregrated Optics, Ministry of Education, and College of Science, Harbin Engineering University, Harbin 150001, China. E-mail: chenyujin@hrbeu.edu.cn*

[b] *College of Materials Science and Chemical Engineering, Harbin Engineering University, Harbin, 150001, China. E-mail: gaopeng@hrbeu.edu.cn, and zhuchunling@hrbeu.edu.cn*

† Electronic Supplementary Information (ESI) available: [Experimental processes, SEM image of MoO_3/PANI hybrids, XRD, SEM, and XPS of MoO_2/Mo_2C-NCNTs, XRD, EELS spectrum for MoS_2/Mo_2C-NCNTs, electrochemical impedance spectroscopy of MoS_2/Mo_2C-NCNTs, and structural characterization of MoS_2 nanoflowers]. See DOI: 10.1039/b000000x/

1 B. Himmemann, P. G. Moses, J. Bonde, K. P. Jørgensen, J. H. Nielsen, S. Horch, I. Chorkendorff and J. K. Nørskov, *J. Am. Chem. Soc.,* 2005, **127**, 5308-5309.

2 T. F. Jaramillo, K. P. Jørgensen, J. Bonde, J. H. Nielsen, S. Horch and Ib Chorkendorff, *Science*, 2007, **317**, 100-102.

3 a) H. Vrubel, D. Merki, X. Hu, *Energy Environ. Sci..*, 2012, **5**, 6136-6144; b) J. Kibsgaard, Z. Chen, B. N. Reinecke andT. F. Jaramillo, *Nat. Mater.,* 2012, **11**, 963-969; c) H. I. Karunadasa, E. Montalvo, Y. J. Sun, M. Majda, J. R. Long and C. J. Chang, *Science*, 2012, **335**, 698-702; d) Z. Chen, D. Cummins, B. N. Reinecke, E. Clark,

M. K. Sunkara and T. F. Jaramillo, *Nano Lett.,* 2011, **11**, 4168-4175; e) J. Bonde, P. G. Moses, T. F. Jaramillo, J. K. Nørskov and I. Chorkendorff, *Faraday Discuss.,* 2009, **140**, 129; f) J. F. Xie, H. Zhang, S. Li, R. X. Wang, X. Sun, M. Zhou, J. F. Zhou, X. W. Lou and Y. Xie, *Adv. Mater.,* 2013, **25**, 5807-5813; g) J. Xie, J. Zhang, S. Li, F. Grote, X. Zhang, H. Zhang, R. Wang, Y. Lei, B. Pan and Y. Xie, *J. Am. Chem. Soc.,* 2013, **135**, 17881-17888; h) S. Zhuo, Y. Xu, W. Zhao, J. Zhang and B. Zhang, *Angew. Chem. Int. Ed.,* 2013, **52**, 8602-8606; i) T. Wang, L. Liu, Z. Zhu, P. Papakonstantinou, J. Hu, H. Liu and M. Li, *Energy Environ. Sci.*, 2013, **6**, 625–633; j) V. W. Lau, A. F. Masters, A. M. Bond and T. Maschmeyer, *Chem. Eur. J.,* 2012, **18**, 8230 – 8239.

4 H. Tributsch, *Berich. Bunsen Gesell.,* 1977, **81**, 361-369.

5 a) A. B. Laursen, S. Kegnæs, S. Dahl, I. Chorkendorff, *Energy Environ. Sci.,* 2012, **5**, 5577-5591; **b)** Y. Peng, Z. Peng, C. Zhong, J. Liu, W. Yu, Z. Yang, Y. Qian, *J. Solid State Chem.*, 2001, **159**, 170–173.

6 a) Y. H. Chang, C. T. Lin, T. Y. Chen, C. L. Hsu, Y. H. Lee, W. Zhang, K. H. Wei and L. J. Li, *Adv. Mater.,* 2013, **25**, 756-760; b) M. A. Lukowski, A. S. Daniel, F. Meng, A. Forticaux, L. Li and S. Jin, *J. Am. Chem. Soc.,* 2013, **135**, 10274-10277; c) F. Meng, J. Li, S. K. Cushing, M. Zhi and N. Wu, *J. Am. Chem. Soc.,* 2013, **135**, 10286-10289; d) A. B. Laursen, P. C. K. Vesborg and I. Chorkendorff, *Chem. Commun.*, 2013, **49**, 4965-4967; e) Q. Xiang, J. Yu and M. Jaroniec, *J. Am. Chem. Soc.,* 2012, **134**, 6575-6578; f) X. Zong, H. Yan, G. Wu, G. Ma, F. Wen, L. Wang and C. Li, *J. Am. Chem. Soc.,* 2008, **130**, 7176-7177; g) Y. Li, H. Wang, L. Xie, Y. Liang, G. Hong and H. Dai, *J. Am. Chem. Soc.,* 2011, **133**, 7296-7299.

7 a) H. Vrubel and X. Hu, *Angew. Chem. Int. Ed.,* 2012, **51**, 12703-12706; b) L. Liao, S. Wang, J. Xiao, X. Bian, Y. Zhang, M. D. Scanlon, X. Hu, Y. Tang, B. H. Liu and H. H. Girault, *Energy Environ. Sci.,* 2014, **7**, 387-392.

8 Q. Wang, Z. Lei, Y. Chen, Q. Ouyang, P. Gao, L. Qi, C. Zhu and J. Zhang, *J. Mater. Chem. A.,* 2013, **1**, 11795-11801.

9 a) N. Chiou, C. M. Lu, J. J. Guan, L. J. Lee and A. J. Epstein, *Nat. Nanotechnol.*, 2007, **2**, 354-357; b) H. Yu, T. Wang, B. Wen, M. Lu, Z. Xu, C. Zhu, Y. Chen, X. Xue, C. Sun and M. Cao, *J. Mater. Chem.*, 2012, **22**, 21679–21685; c) R. J. Tseng, J. X. Huang, J. Y. Ouyang, R. B. Kaner and Y. Yang, *Nano Lett.*, 2005, **5**, 1077-1080.

10 Y. Yin, R. M. Rioux, C. K. Erdonmez, S. Hughes, G. A. Somorjai and A. P. Alivisatos, *Science,* 2004, **304**, 711–714.

11 G. Eda, H. Yamaguchi, D. Voiry, T. Fujita, M. Chen and M. Chhowalla, *Nano Lett.,* 2011, **11**, 5111–5116.

12 W. Chen, C. Wang, K. Sasaki, N. Marinkovic, W. Xu, J. Muckerman, Y. Zhu, R. Adzic, *Energy & Environmental Science*, 2013, **6**, 943-951.

13 C.J. Ge, P. Jiang, W. Cui, Z.H. Pu, Z.C. Xing, A. M. Asiri, A. Y. Obaid, X. P. Sun, J. Tian, *Electrochimica Acta*,2014, **134**,182–186.